AGU PUBLICATIONS

Geophysical Research Letters

RESEARCH LETTER
10.1002/2014GL063002

Key Points:
- A *P* wave-based method for an on-site earthquake early warning system is proposed
- Three parameters are jointly used for the ground shaking prediction
- The combination of three parameters improves the robustness of the system

Supporting Information:
- Texts S1–S5, Figures S1–S9, and Tables S1–S4

Correspondence to:
S. Colombelli,
simona.colombelli@unina.it

Citation:
Colombelli, S., A. Caruso, A. Zollo, G. Festa, and H. Kanamori (2015), A *P* wave-based, on-site method for earthquake early warning, *Geophys. Res. Lett.*, *42*, 1390–1398, doi:10.1002/2014GL063002.

Received 29 DEC 2014
Accepted 10 FEB 2015
Accepted article online 13 FEB 2015
Published online 13 MAR 2015

A *P* wave-based, on-site method for earthquake early warning

S. Colombelli[1], A. Caruso[1], A. Zollo[1], G. Festa[1], and H. Kanamori[2]

[1]Department of Physics, University of Naples Federico II, Naples, Italy, [2]Division of Earth and Planetary Science, California Institute of Technology, Pasadena, California, USA

Abstract A new strategy for a *P* wave-based, on-site earthquake early warning system has been developed and tested on Japanese strong motion data. The key elements are the real-time, continuous measurement of three peak amplitude parameters and their empirical combination to predict the ensuing peak ground velocity. The observed parameters are compared to threshold values and converted into a single, dimensionless variable. A local alert level is issued as soon as the empirical combination exceeds a given threshold. The performance of the method has been evaluated by applying the approach to the catalog of Japanese earthquake records and counting the relative percentage of successful, missed, and false alarms. We show that the joint use of three peak amplitude parameters improves the performance of the system as compared to the use of a single parameter, with a relative increase of successful alarms of about 35%. The proposed methodology provides a more reliable prediction of the expected ground shaking and improves the robustness of a single-station, threshold-based earthquake early warning system.

1. Introduction

The concept of earthquake early warning systems (EEWSs) is nowadays popular, and their potential to mitigate the destructive effects of earthquakes is well recognized. EEWSs are real-time, seismic monitoring systems able to detect an ongoing earthquake and provide a warning to a target area, before the arrival of the most destructive waves. In Japan, EEWSs were developed since 1960s in conjunction with the development of high-speed railway systems, and *Nakamura*'s [1988] urgent earthquake detection and alarm system played an important role. The EEW system developed by the National Research Institute for Earth Science and Disaster Prevention (NIED) and the Japan Meteorological Agency are most widely used in the public since 2007 [*Odaka et al*., 2003; *Horiuchi et al*., 2005; *Hoshiba et al*., 2011]. Operational EEW platforms providing public warning are also available in Mexico [*Espinosa-Aranda et al*., 2009], Romania [*Böse et al*., 2007], Turkey [*Alcik et al*., 2009], and Taiwan [*Wu and Teng*, 2002; *Wu and Zhao*, 2006]. Rapid progress has been recently made in California, and the project is now moving toward implementation of a statewide EEWS [*Böse et al*., 2013; *Kuyuk et al*., 2014]. Other EEWSs are under development and testing in Southern Italy [*Zollo et al*., 2009; *Satriano et al*., 2010; *Zollo et al*., 2014] and China [*Peng et al*., 2011], while feasibility studies are in progress for the Iberian Peninsula [*Carranza et al*., 2013] and South Korea [*Zollo et al*., 2013].

In a *regional* EEWS the seismic network is located nearby the source area, while target sites to be alerted are far away from it. In this configuration, the relevant source parameters (event location and magnitude) are estimated from the early portion of recorded signals and are used to predict the expected ground shaking (peak ground velocity, PGV, and peak ground acceleration, PGA) at the target sites through empirical ground motion prediction equations. The *on-site* configuration consists of a single sensor or of an array of sensors deployed in the proximity of the target structure to be alerted. Here the initial *P* wave motion recordings are used to predict the ensuing peak ground motion at the same site, without necessarily estimating the earthquake location and magnitude. Combined approaches have been recently proposed [*Zollo et al*., 2010; *Colombelli et al*., 2012a]. These are based on the joint use of locally measured parameters and predicted ground motion values at regional scale and are aimed at providing reliable and fast estimates of source parameters and of the potential damage zone.

Whichever configuration is adopted, an alert is generally issued when the predicted ground motion exceeds a predefined threshold. In EEWS the strong motion is generally described by a single parameter (PGA or PGV) which can be related to the damage and/or to the perceived shaking. Many authors demonstrated that the maximum amplitude of the initial *P* wave displacement (measured within 3 s) can be used as a proxy for

predicting PGV at the same site [*Kanamori*, 2005; *Wu and Kanamori*, 2005, 2008; *Zollo et al*., 2010]. Here we propose and test an optimized strategy for a single-station, threshold-based EEWS, using a set of moderate-to-large Japanese earthquakes. The methodology we propose is straightforward and robust and is essentially based on two key elements. The first one is the continuous measurement of three peak amplitude parameters (the initial peak of displacement, P_d, velocity, P_v, and acceleration, P_a) on the vertical component of ground motion recordings. Following the concept of the expanded *P* wave time window (PTW), the real-time measurements are here progressively performed starting from the *P* wave onset and continuously updated as long as the ground motion is recorded. The second key element of the proposed methodology is a use of an empirical combination of the three ground motion parameters for predicting the ensuing PGV at the same site.

2. Database and Method

The database we used consists of 76 Japanese events in the magnitude range $4.0 \leq M \leq 9.0$ (Text S1 in the supporting information). Among them, 73 events were used for deriving the empirical correlations and for setting the threshold values and three earthquakes were used for validation and scenario studies (Tables S1 and S2 in the supporting information). For each event, we selected the three-component, strong motion accelerometer records, available in the distance range *R* 0–500 km, for a total of 12,792 three-component records (Text S1 in the supporting information). Figure 1a shows the distribution of selected events and used stations. Figures 1b and 1c show the magnitude and distance histograms, for the calibration and the validation data set.

At each time along the seismogram, we measure P_d, P_v, and P_a on the vertical component of ground motion recordings (Text S2 in the supporting information) and associate them with a fuzzy variable $W_x(t)$, defined as

$$\begin{aligned} W_x(t) &= 0 && \text{if } P_x(t) \leq P_{xL} \\ W_x(t) &= 1/3\,[(P_x(t) - P_{xL}) \,/\, (P_{xH} - P_{xL})] && \text{if } P_{xL} < P_x(t) < P_{xH} \\ W_x(t) &= 1/3 && \text{if } P_x(t) \geq P_{xH} \end{aligned}$$

where the subscript *x* stands for displacement (*d*), velocity (*v*), or acceleration (*a*), respectively, and P_{xL} and P_{xH} indicate the lower and higher threshold values for the parameter *x*. $W_x(t)$ is computed at each time and is locked at the corresponding value until a larger value is encountered. As a result, $W_x(t)$ is a monotonically increasing stepladder-like function, as shown in Figure 1d. We then sum up the values of W_d, W_v, and W_a to define a single logical variable W_t, which is now used for warning declaration (Figure 1d, bottom). Instead of using one parameter with a single preset threshold, here we are combining three ground motion parameters, accounting for the uncertainty of the empirical scaling relationships. The use of the fuzzy variable is a simplified, although arbitrary, way to convert a single-parameter, binary, decision scheme into a multivariable, continuous, alert system. With the proposed definition of W_d, W_v, and W_a, the three ground motion quantities equally contribute to the final shaking prediction.

To define the thresholds for warning, we converted a given instrumental intensity (I_{MM}) to PGV [*Wald et al*., 1999] and extracted the values of P_d, P_v, and P_a associated to such a PGV value, through empirical correlations between these three parameters and the PGV (Figure 1e and Text S3 and Figure S1 in the supporting information). We used two intensity levels $I_{MM} = V$ (i.e., PGV = 3.4 cm/s) and $I_{MM} = VII$ (i.e., PGV = 16 cm/s), which correspond to the "light-to-moderate" and "strong-to-very strong" transitions on the perceived shaking and on the produced damage [*Wald et al*., 1999, table description]. For each intensity threshold value, the threshold values on the amplitude parameters are obtained from intersections of the threshold PGV with the empirical correlations ±1 standard deviation (Figures 1e and 1f and Figure S1 and Table S3 in the supporting information). For the derivation of the empirical scaling relationships, we avoided the *S* wave contamination by terminating the time window for P_d, P_v, and P_a measurement at the expected arrival of the *S* waves.

As system output, we defined four different alert levels (e.g., W_t versus PGV diagram; Figure S2 in the supporting information) based on a threshold on W_t, hereinafter denoted as W_t*: successful alarm (SA), successful no alarm (SNA), false alarm (FA), and missed alarm (MA). The threshold value of W_t on the PGV versus W_t plot controls the overall performance of the system, with an intrinsic trade-off between FA and MA (Figure 1g). High values of W_t* generally provide a small number of FA but may frequently generate MA. On the contrary, small values of W_t* are expected to reduce the MA but consequently to increase the

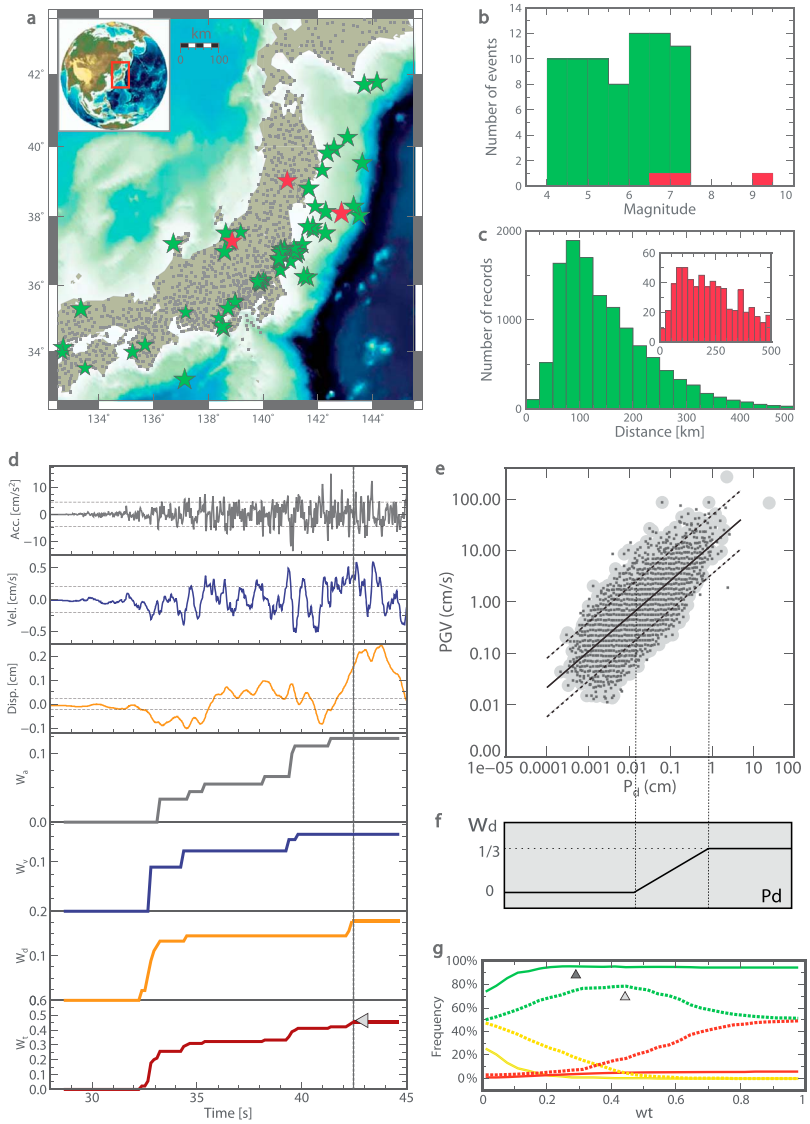

Figure 1. Data and method. (a) The map shows the distribution of stations (gray dots) and the epicentral location of the selected events. Green stars are the earthquakes used for the calibration, while red stars are the scenario events. The size of the star is proportional to the magnitude. (b) Histogram of the number of earthquakes as a function of magnitude, for the calibration data set (green) and for the scenario studies (red). (c) Distribution of records as a function of distance, for the calibration (green) and for the scenario events (red). (d) From top to bottom, an example of the vertical component of acceleration (black), velocity (blue), and displacement (orange) signals. The initial peak amplitude parameters P_d, P_v, and P_a are measured as the absolute maximum of displacement waveform on the early portion of *P* wave. The threshold values (for the intensity $I_{MM} = V$) on each parameter are schematically shown as a black, dashed line on each record. Examples of W_a, W_v, and W_d as a function of time are also shown with a solid black, blue, and orange lines, respectively. Each step on W_a, W_v, and W_d corresponds to an increase of the peak amplitude parameters (as absolute value) on the ground motion records. Finally, the bottom plot shows the cumulative logical variable W_t as a function of time (purple curve). Here the gray rotated triangle shows the threshold value W_t^* used for warning declaration ($W_t^* = 0.45'$ in this case). (e) Data distribution and empirical relationships between P_d and PGV. The background, gray circles represent the whole data set, while the small, black squares are data used for calibrating the scaling relationships (Text S3 in the supporting information). The solid black line is the best fit line, while dashed lines are the standard error of regression. (f) Example of W_d definition. The observed P_d parameter is compared to its threshold value and converted into a dimensionless variable, named W_d, which is equal to 0 in the region below the lower threshold to 1/3 in the region above the higher threshold and linearly increases between 0 and 1/3 in the intermediate region. (g) Calibration curves: the figure shows the number of MA (red line), FA (yellow line), and total successful alarms (including SA and SNA, green line) as a function of W_t. The solid lines are referred to the higher-intensity threshold ($I_{MM} = VII$), while the dashed lines are associated to the lower intensity threshold ($I_{MM} = V$). The threshold values of W_t are marked as a triangle on the successful alarm curves (light gray for the lower intensity and dark gray for the higher-intensity threshold).

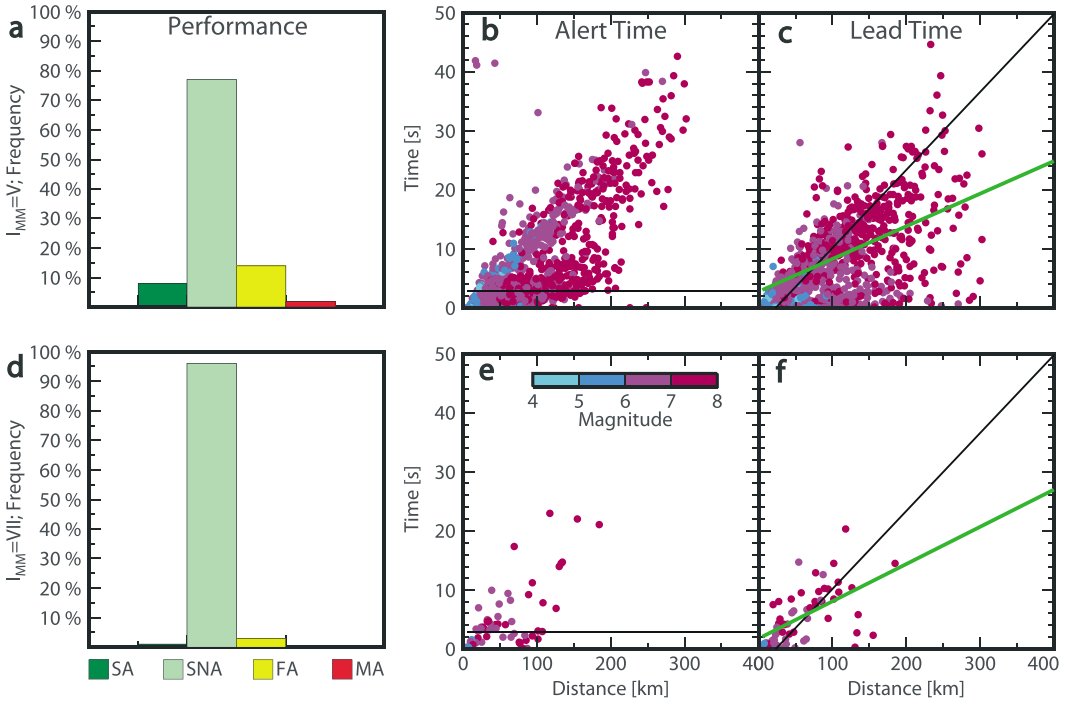

Figure 2. Overall performance of the methodology. (a, d) The histograms show the performance of the system in terms of SA (dark green bar), SNA (light green bar), FA (yellow bar), and MA (red bar) for the two intensity levels. (b, e) Alert times as a function of distance. The black line is the theoretical alert time for the fixed PTW on-site system (3 s). (c, f) Lead times as a function of distance. The black line is the theoretical lead time for the fixed PTW on-site system (*S-P* arrival time difference at each site), while the green line is the best fit regression of the observed lead time as a function of distance. In Figures 2b, 2c, 2e, and 2f the color scale represents the earthquake magnitude.

occurrence of FA. After analyzing the number of missed, false, and successful alarms as a function of W_t, for the present work we chose the optimal value of W_t* by maximizing the total percentage of successful alarms.

3. Application and Results

The performance of the proposed EEWS is evaluated by counting the percentage of successful alarms (SA and SNA), FA and MA. Figure 2 shows the overall performance of the system for the two intensity levels chosen in terms of alert percentages (Figures 2a and 2d) and in terms of alert and lead times (Figures 2b, 2c, 2e, and 2f). The alert time is defined as the time elapsed between the arrival of the *P* wave and the alert declaration (i.e., when W_t exceeds the threshold). The lead time is the time available from the warning declaration to the instant at which PGV exceeds the threshold value. For both the intensity thresholds, the joint use of P_d, P_v, and P_a significantly improves the performance of the system, as compared to the independent use of single-amplitude parameters. With the proposed approach we found, indeed, a high percentage (more than 85%) of successful alarms (including both SA and SNA), a small number of FA (about 14%), and a very low percentage of MA (about 1%). For comparison, Figure S3 in the supporting information shows the performance of the system when the three amplitude parameters are independently used. For single parameters, the percentage of FA still remains too high especially for the lower intensity threshold (about 50%), and therefore, none of the three parameters alone can be considered sufficiently reliable for warning declaration.

Beyond the correct alert declaration, the ability to rapidly provide warning is also a crucial feature of an EEWS. In terms of timing performances the proposed approach may require longer signal portions for warning declaration, as compared to the standard on-site approaches. Nevertheless, the methodology is able to provide sufficient warning times, as illustrated in the plot of alert times and lead times as a function of distance (Figures 2b, 2c, 2e, and 2f). We observe that alert times and lead times increase with increasing distance and magnitude (Figures 2b, 2c, 2e, and 2f). On average, at short distance from the source (< 25 km),

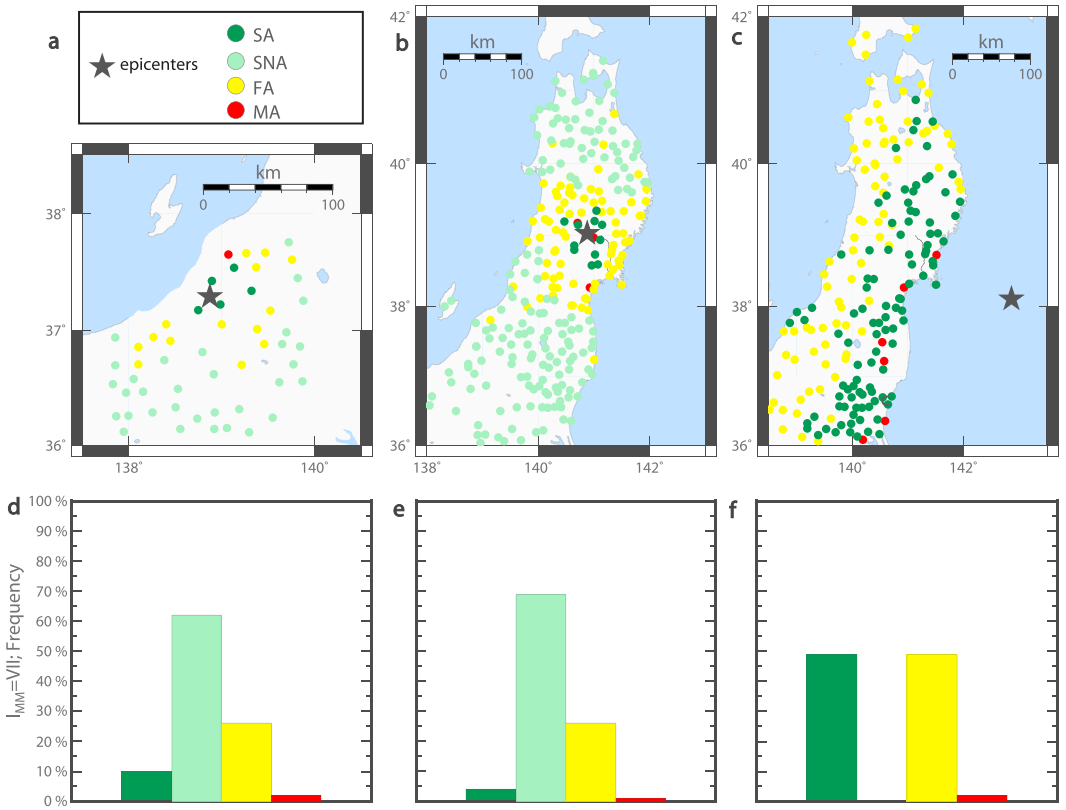

Figure 3. Scenario events and relative histogram of the performance, for the higher-intensity threshold (I_{MM} = VII). Map of the alert distribution for (a) the 2004 *M* 6.8 Chuetsu event, (b) the 2008 *M* 7.2. Miyagi-Iwate earthquake, and (c) the offshore 2011 *M* 9.0 Tohoku-Oki event. Small colored circles represent the stations used, and the black star is the earthquake epicenter. (d–f) Histograms of the alert levels for the three scenario events. For all panels, the color scheme is the same as used in Figure 2 and is also explained in the legend.

the available lead time is 3–4 s while 5–7 s are available at intermediate distances (25–75 km). At a distance of 100 km, the lead time is about 8 s; 15 s are available at 200 km and 25 s at 400 km.

We also evaluated the performance of the system when limited PTWs are used, i.e., when the parameter computation is stopped at the expected arrival time of *S* waves (Figure S4 in the supporting information). Generally, the use of limited PTWs reduces the number of FA, but a consequent increase of the number of MA is observed.

We analyzed the performance of the proposed methodology for three scenario earthquakes (Figure 3), which were not used to calibrate the empirical relationships. We analyzed a small-to-moderate inland earthquake (the 2004, *M* 6.8 Chuetsu event, Figures 3a and 3d), a moderate-to-large inland earthquake (the 2008, *M* 7.2. Miyagi-Iwate earthquake, Figures 3b and 3e), and the offshore *M* 9.0 2011, Tohoku-Oki event (Figures 3c and 3f). For the scenario analysis, we focus on the higher-intensity threshold level (I_{MM} = VII), while the performance for the lower intensity value is shown in the supporting information (Figure S5). For the two smallest earthquakes we found a relatively large percentage of total successful alarms (about 70–75%), an average percentage of FA around 25%, and an extremely low number of MA (< 2%). For the 2011 *M* 9.0, Tohoku-Oki earthquake, successful and FA are almost balanced around 49%, while the percentage of MA is again very small (< 2%).

4. Discussion and Conclusive Remarks

The proposed EEW methodology is based on the real-time, continuous measurement of three peak amplitude parameters which are empirically combined for the prediction of the expected shaking at the same site. Acceleration, velocity, and displacement provide a complementary image of the spectral content of the source, whose highest frequencies are mostly associated to finer details of the rupture process and

wave propagation, while the low-frequency content is mainly determined by the seismic moment. The overall statistics confirmed that the performance of the system significantly improves when the combination of the three parameters is used, with a significant increase of successful alarms and a substantial reduction of false alarms. The combination of three different parameters provides a broader insight into the ongoing phenomena, while keeping the methodology as simple as possible. Compared with the standard on-site methodologies, this approach is likely to provide reliable warnings and more robust prediction of potential earthquake damaging effects.

In the proposed approach, the initial amplitude parameters are continuously measured on the ground motion recordings and the use of limited *P* wave windows has been replaced by expanded PTWs. Standard approaches to EEW may significantly underestimate very large events. The empirical regression relationships between amplitude parameters and magnitude are indeed calibrated on short portion of *P* wave signals and saturate beyond a magnitude 7–7.5 [*Kanamori*, 2005; *Rydelek and Horiuchi*, 2006; *Rydelek et al*., 2007; *Zollo et al*., 2007; *Festa et al*., 2008]. This saturation is due to the *P* signal emitted from a too small portion of the fault plane, whose behavior in terms of slip and stress release may not correlate with the final average behavior of the whole rupture. When an earthquake rupture extends over hundreds of kilometers on the fault, the large asperities possibly encountered far away from the hypocenter may control the total amount of stress release and the radiated energy. The analysis of strong motion data of the M_w 9.0 Tohoku-Oki earthquake confirmed that a larger PTW is necessary to properly estimate the size of the ongoing event [*Colombelli et al*., 2012b, 2014]. The possibility of expanding the observation time window allows for capturing longer portions of the rupture process and lower frequencies radiated from the source, thus possibly avoiding the earthquake magnitude underestimation.

In practice, a possible risk when expanding the PTW is the inclusion of *S* waves, whose amplitude, if not properly considered, may lead to an overestimation of the predicted ground shaking level. The use of the vertical component of ground motion recordings, in principle, minimizes the *S* wave contamination on the *P* wave amplitude measurement. However, in those regions where extensional or compressional tectonics is dominant, a large portion of the *S* wave amplitude may contaminate the vertical component of ground motion. For example, in the case of Japan, the *S* wave amplitude on the vertical component is about one third of the total amplitude (Figure S6 in the supporting information). In order to mitigate this effect, algorithms for the automatic *S* wave detection and picking could be used, based on the real-time polarization analysis on the three-component seismogram [e.g., *Rosenberger*, 2010; *Amoroso et al*., 2012].

While accurate estimations of the *S* wave arrival time are not required for EEW applications, an approximate estimation of the event magnitude and distance would be a relevant piece of information to be provided. In particular, an estimation of the available lead time can be inferred by the earthquake distance from the recording station. A rough estimate of the hypocentral distance and the magnitude can be empirically estimated at each site from P_d, P_v, and P_a as described in Text S4 in the supporting information. As an example, Figure S7 in the supporting information shows how magnitude and distance could be approximately estimated using the three observed ground motion parameters for the *M* 7.2 Iwate-Miyagi earthquake. The estimated magnitude values are distributed around the true value, although the scatter is quite large (±1 standard error). Similarly, the trend between predicted and observed log distance is almost well reproduced, up to distances of about 300 km. The combined use of the three attenuation relationships (P_d, P_v, and P_a as a function of magnitude and distance) can be extremely useful for single-station systems, where little constraint on the earthquake source or location and magnitude is available in real time. The proposed methodology can provide an approximate estimate of magnitude, epicentral distance, and expected lead time. These parameters can be used for a first-order discrimination between the case of a small-magnitude, faraway event, and the occurrence of a large earthquake nearby the recording station.

The performance of the system significantly changes when limited (i.e., up to the *S* wave first arrival) or unlimited PTWs are considered. Figure S8 in the supporting information shows the performance for the scenario cases, when limited time windows are used. As expected, when no time limit is imposed, the incidence of FA increases, with respect to the case of limited PTWs. The increase of FA, however, is balanced by a substantial reduction of MA, which is, indeed, the most critical issue for an EEWS. This is especially true for the case of the 2011, M_w 9.0, Tohoku-Oki earthquake, for which the percentage of MA decreases from about 50% to only 2%, when unlimited time windows are used.

One of the main advantages of the proposed methodology is that, in principle, FA or MA can be prioritized at the user's discretion. Following the calibration curves of Figure 1g, for example, the percentage of FA can be reduced by choosing a high W_t* value, with a consequent little increase of MA. On the contrary, for those applications in which FA is more tolerable, while MA should be avoided, lower W_t* values are to be preferred. The specific tuning of W_t* values and the development of a robust, *S* wave discriminator are the most effective ways to improve the performance of the proposed approach. In principle, if the *S* wave contamination on the vertical component of ground motion could be eliminated, the incidence of FA could be reduced, while MA could be avoided through a proper setting of the warning threshold.

In terms of timing performance, the proposed methodology may require shorter or longer signal portions for warning declaration, as compared to the standard approaches based on measures in a fixed and short PTW. For instance, if 3 s of *P* wave signal are used for parameter estimation, the alert time depends on neither the source-to-receiver distance nor the earthquake magnitude (Figures 2b and 2e). In the proposed approach, instead, both distance and magnitude play a key role. We found that alert times are around 1–2 s for small-to-moderate events recorded at small epicentral distances (i.e., for magnitude between 4 and 5 within 100 km), while longer PTWs are required in case of large events recorded at large distances (20–30 s for magnitude 9 events, recorded at 300 km). This result is consistent with the recent observations of *Colombelli et al*. [2014] who measured the logarithm of P_d over progressively expanding PTWs and found that it starts with small values and then progressively increases with time, until a plateau value is reached. The greater the magnitude, the longer the time needed for P_d to reach its final value. Thus, in the proposed approach, the warning can be declared within a very short time window for small-to-moderate events, while longer *P* wave signals are needed to properly predict the expected shaking for large events.

As for the lead times, the plot of Figures 2c and 2f shows a clear dependency on both distance and magnitude, as confirmed by the best fit regression line (green line) and by the color scale. As for the distance dependency, this result is not surprising, since the lead time is approximately given by the *S-P* wave traveltime difference. At very short distances from the source our observed lead times are slightly longer than the theoretical values, with about 3 to 4 s of warning available within 25 km from the epicenter. At larger distances, instead, our lead times are generally smaller than the theoretical values, with about 8 s of lead time at a distance of 100 km and about 15 s at 200 km. Assuming a 20 km spacing between the stations (as in the case of Japan network), 1 s of lead time is computed at a distance of 25 km while more than 20 s of warning are expected at 100 km away from the source [*Kuyuk and Allen*, 2013]. For comparison, the theoretical lead time as a function of distance is shown with a black line. The dependency of lead times on magnitude can be explained in terms of source process and of propagation effects. For large events, indeed, the source process has a longer duration and a late peak in the moment rate function is expected. In addition, magnitude generally increases with distance in our database, with the largest events mostly occurring offshore. As a consequence, the strongest ground shaking can be associated either to later slip episodes or to the arrival of later phases.

The application of the proposed methodology to the *M* 9.0 Tohoku-Oki event yielded an anomalous high percentage of FA (about 49%), relative to the other cases. Probably, because of the extremely large size, long-period waves with long duration dominated, and the warning algorithm, calibrated with smaller magnitudes, fails. Since long-period waves have significant effects on large structures, it will be important to develop a separate warning scheme for long-period motions from extremely large earthquakes. To this end, not only the initial amplitude but also the dominant period needs to be monitored. Furthermore, an approximate estimate of the event magnitude as described in Text S4 in the supporting information could also be a relevant piece of information to provide. In our application, we note that, however, all of these FAs are associated with a ground shaking amplitude effectively perceived and experimented by population. This mitigates the negative impact of false alarms and cry wolf syndrome due to the effective experience of earthquake shaking as a consequence of the alert.

The proposed methodology is conceived to operate as a single-station, threshold-based, EEWS and is expected to improve the reliability of an on-site system, where no information or constraint on the earthquake source is available in real time. A practical strategy for the proposed approach could be to declare the first warning as soon as the lower intensity threshold is exceeded and then to confirm (or possibly cancel) the previous alert, if the higher-intensity threshold is reached. Although conceived for a single-station approach, the methodology proposed here could be easily integrated in a network-based EEW platform. The real-time, local

measurement of *P* wave amplitude can be used to upgrade or confirm the information coming from the regional-scale system. Following the approach proposed by *Zollo et al.* [2010] and *Colombelli et al.* [2012a], locally observed and predicted amplitude parameters can be jointly used for the definition of a local alert level and for rapid mapping of the area where the highest damage is expected to occur.

Another practical aspect to consider when applying the proposed methodology is the possible influence of site effects, which may produce local, systematic amplification/attenuation of the perceived shaking (Text S5 in the supporting information). A detailed analysis on the role of site effects is needed when calibrating the proposed methodology for a specific region.

The proposed approach for EEW could be suitable to Japan and to other high seismic risk countries in the world, where a dense network of accelerometers is developed over the whole territory. In particular, the methodology can be useful for those cases where "front detection" systems are adopted, such as Mexico City (seismic alert system [*Espinosa-Aranda et al.*, 1995]) or along the Atlantic coast of the Iberian Peninsula, where it could provide rapid and reliable alarms with information about the potential damaging effects of the event.

Acknowledgments

We acknowledge the Japanese National Research Institute for Earth Science and Disaster Prevention (NIED) for making the Kik-Net and K-net strong motion data accessible through website (http://www.kyoshin.bosai.go.jp/). This work was funded by the University of Naples Federico II and AMRA s.c.a r.l. in the framework of EU-FP7 REAKT project (Strategies and Tools for Real-Time Earthquake Risk Reduction) funded by the European Community via the Seventh Framework Program for Research (FP7), contract 282862. We are grateful to Matteo Picozzi for his constructive comment during the work and wish to thank Serdar H. Kuyuk and an anonymous reviewer for the careful revision of our manuscript.

The Editor thanks Rongjiang Wang and Huseyin Kuyuk for their assistance in evaluating this paper.

References

Alcik, H., O. Ozel, N. Apaydin, and M. Erdik (2009), A study on warning algorithms for Istanbul earthquake early warning system, *Geophys. Res. Lett.*, *36*, L00B05, doi:10.1029/2008GL036659.

Amoroso, O., N. Maercklin, and A. Zollo (2012), S-wave identification by polarization filtering and waveform coherence analyses, *Bull. Seismol. Soc. Am.*, *102*(2), 854–861, doi:10.1785/0120110140.

Böse, M., C. Ionescu, and F. Wenzel (2007), Earthquake early warning for Bucharest, Romania: Novel and revised scaling relations, *Geophys. Res. Lett.*, *34*, L07302, doi:10.1029/2007GL029396.

Böse, M., et al. (2013), CISN ShakeAlert: An earthquake early warning demonstration system for California, in *Early Warning for Geological Disasters—Scientific Methods and Current Practice*, edited by F. Wenzel and J. Zschau, pp. 49–69, Springer, Berlin, doi:10.1007/978-3-642-12233-0_3.

Carranza, M., E. Buforn, S. Colombelli, and A. Zollo (2013), Earthquake early warning for southern Iberia: A *P* wave threshold-based approach, *Geophys. Res. Lett.*, *40*, 4588–4593, doi:10.1002/grl.50903.

Colombelli, S., O. Amoroso, A. Zollo, and H. Kanamori (2012a), Test of a threshold-based earthquake early warning using Japanese data, *Bull. Seismol. Soc. Am.*, *102*, 1266–1275, doi:10.1785/0120110149.

Colombelli, S., A. Zollo, G. Festa, and H. Kanamori (2012b), Early magnitude and potential damage zone estimates for the great Mw 9 Tohoku-Oki earthquake, *Geophys. Res. Lett.*, *39*, L22306, doi:10.1029/2012GL053923.

Colombelli, S., A. Zollo, G. Festa, and M. Picozzi (2014), Evidence for a difference in rupture initiation between small and large earthquakes, *Nat. Commun.*, *5*, 3958, doi:10.1038/ncomms4958.

Espinosa-Aranda, J. M., A. Jimenez, G. Ibarrola, F. Alcantar, A. Aguilar, M. Inostroza, and S. Maldonado (1995), Mexico city seismic alert system, *Seismol. Res. Lett.*, *66*(6), 42–53.

Espinosa-Aranda, J. M., A. Cuellar, A. Garcia, G. Ibarrola, R. Islas, S. Maldonado, and F. H. Rodriguez (2009), Evolution of the Mexican seismic alert system (SASMEX), *Seismol. Res. Lett.*, *80*, 694–706.

Festa, G., M. Lancieri, and A. Zollo (2008), Magnitude estimation from early radiated energy, *Geophys. Res. Lett.*, *35*, L22307, doi:10.1029/2008GL035576.

Horiuchi, S., H. Negishi, K. Abe, A. Kamimura, and Y. Fujinawa (2005), An automatic processing system for broadcasting system earthquake alarms, *Bull. Seismol. Soc. Am.*, *95*, 347–353.

Hoshiba, M., K. Iwakiri, N. Hayashimoto, T. Shimoyama, K. Hirano, Y. Yamada, Y. Ishigaki, and H. Kikuta (2011), Outline of the 2011 off the Pacific coast of Tohoku Earthquake (Mw 9.0)—Earthquake early warning and observed seismic intensity, *Earth Planets Space*, *63*, 547–551.

Kanamori, H. (2005), Real-time seismology and earthquake damage mitigation, *Annu. Rev. Earth Planet. Sci.*, *33*, 195–214, doi:10.1146/annurev.earth.33.092203.122626.

Kuyuk, H. S., and R. M. Allen (2013), Optimal seismic network density for earthquake early warning: A case study from California, *Seismol. Res. Lett.*, *84*(6), 946–954.

Kuyuk, H. S., R. M. Allen, H. Brown, M. Hellweg, I. Henson, and D. Neuhauser (2014), Designing a network-based earthquake early warning algorithm for California: ElarmS-2, *Bull. Seismol. Soc. Am.*, *104*, 162–173, doi:10.1785/0120130146.

Nakamura, Y. (1988), On the urgent earthquake detection and alarm system (UrEDAS), in *Proceedings of Ninth World Conference on Earthquake Engineering, Paper# 13-2-12*, vol. VII, pp. 673–678, Tokyo-Kyoto, 2–9 Aug.

Odaka, T., K. Ashiya, S. Tsukada, S. Sato, K. Ohtake, and D. Nozaka (2003), A new method of quickly estimating epicentral distance and magnitude from a single seismic record, *Bull. Seismol. Soc. Am.*, *93*, 526–532.

Peng, H. S., Z. L. Wu, Y. M. Wu, S. M. Yu, D. N. Zhang, and W. H. Huang (2011), Developing a prototype earthquake early warning system in the Beijing capital region, *Seismol. Res. Lett.*, *82*, 394–403.

Rosenberger, A. (2010), Real-time ground-motion analysis: Distinguishing P and S arrivals in a noisy environment, *Bull. Seismol. Soc. Am.*, *100*, 1252–1262.

Rydelek, P., and S. Horiuchi (2006), Is earthquake rupture deterministic?, *Nature*, *442*, E5–E6, doi:10.1038/nature04963.

Rydelek, P., C. Wu, and S. Horiuchi (2007), Comment on "Earthquake magnitude estimation from peak amplitudes of very early seismic signals on strong motion records" by Aldo Zollo, Maria Lancieri, and Stefan Nielsen, *Geophys. Res. Lett.*, *34*, L20302, doi:10.1029/2007GL029387.

Satriano, C., L. Elia, C. Martino, M. Lancieri, A. Zollo, and G. Iannaccone (2010), PRESTo, the earthquake early warning system for Southern Italy: Concepts, capabilities and future perspectives, *Soil Dyn. Earthquake Eng.*, *31*(2), 137–153, doi:10.1016/j.soildyn.2010.06.008.

Wald, D. J., V. Quitoriano, T. H. Heaton, and H. Kanamori (1999), Relationships between peak ground acceleration, peak ground velocity and modified Mercalli intensity in California, *Earthquake Spectra*, *15*, 557–564.

Wu, Y. M., and H. Kanamori (2005), Experiment of an on-site method for the Taiwan Early Warning System, *Bull. Seismol. Soc. Am.*, *95*, 347–353, doi:10.1785/0120040097.

Wu, Y. M., and H. Kanamori (2008), Development of an earthquake early warning system using real-time strong motion signals, *Sensors*, *8*, 1–9.
Wu, Y. M., and T. L. Teng (2002), A virtual sub-network approach to earthquake early warning, *Bull. Seismol. Soc. Am.*, *92*, 2008–2018.
Wu, Y. M., and L. Zhao (2006), Magnitude estimation using the first three seconds P-wave amplitude in earthquake early warning, *Geophys. Res. Lett.*, *33*, L16312, doi:10.1029/2006GL026871.
Zollo, A., M. Lancieri, and S. Nielsen (2007), Reply to comment by P. Rydelek et al. on "Earthquake magnitude estimation from peak amplitudes of very early seismic signals on strong motion records", *Geophys. Res. Lett.*, *34*, L20303, doi:10.1029/2007GL030560.
Zollo, A., et al. (2009), Earthquake early warning system in southern Italy: Methodologies and performance evaluation, *Geophys. Res. Lett.*, *36*, L00B07, doi:10.1029/2008GL03668.
Zollo, A., O. Amoroso, M. Lancieri, Y. M. Wu, and H. Kanamori (2010), A threshold-based earthquake early warning using dense accelerometer networks, *Geophys. J. Int.*, *183*, 963–974.
Zollo, A., A. Emolo, S. Colombelli, L. Elia, G. Festa, C. Martino, and M. Picozzi (2013), PRESTo—Probabilistic and evolutionary early warning system: Concepts, performances, and case studies, Abstract S41A AGU2013-2407 presented at 2013 Fall Meeting, AGU, San Francisco, Calif.
Zollo, A., S. Colombelli, L. Elia, A. Emolo, G. Festa, G. Iannaccone, C. Martino, and P. Gasparini (2014), An integrated regional and on-site Earthquake Early Warning System for Southern Italy: Concepts, methodologies and performances, in *Early Warning for Geological Disasters—Scientific Methods and Current Practices*, edited by F. Wenzel and J. Zschau, pp. 117–137, Springer, Berlin.